

Journal of Materials Chemistry A

Accepted Manuscript



This is an *Accepted Manuscript*, which has been through the Royal Society of Chemistry peer review process and has been accepted for publication.

Accepted Manuscripts are published online shortly after acceptance, before technical editing, formatting and proof reading. Using this free service, authors can make their results available to the community, in citable form, before we publish the edited article. We will replace this *Accepted Manuscript* with the edited and formatted *Advance Article* as soon as it is available.

You can find more information about *Accepted Manuscripts* in the [Information for Authors](#).

Please note that technical editing may introduce minor changes to the text and/or graphics, which may alter content. The journal's standard [Terms & Conditions](#) and the [Ethical guidelines](#) still apply. In no event shall the Royal Society of Chemistry be held responsible for any errors or omissions in this *Accepted Manuscript* or any consequences arising from the use of any information it contains.

Scalable Synthesis of Sulfur Nanosponge Cathode for Lithium-Sulfur Battery with Improved Cyclability

Junjie Niu, Akihiro Kushima, Mingda Li, Ziqiang Wang, Wenbin Li, Chao Wang and Ju Li*

Department of Nuclear Science and Engineering and Department of Materials Science and Engineering, Massachusetts Institute of Technology, Cambridge, Massachusetts 02139, USA

*Corresponding author: liju@mit.edu

Although lithium-sulfur batteries exhibit a high initial capacity, production cost and lack of cyclability are major limitations. Here we report a liquid-based, low-cost and reliable synthesis method of lithium-sulfur composite cathode with improved cyclability. An open network of Conductive Carbon Black nanoparticles (Cnet) is infused with sulfur (Snet) to form sponge-like networks (Cnet + Snet). Initially, Snet is open to the outside, allowing liquid electrolyte to infiltrate and impart Snet Li^+ conductivity. During lithiation, Cnet could accommodate the volume expansion of Snet without largely losing electrical contact. During delithiation, the carbon nanoparticles would preferably flocculate on outer surface due to polysulfide dissolution and depletion of sulfur, to form a passivation layer that still allows Li^+ exchange, but preventing more polysulfides from getting out, thus slowing the leaching of polysulfides into bulk electrolyte liquid. The plausibility of carbonaceous passivation layer was checked using an extra carbon deposition layer to achieve an improved performance of ~ 400 mAh/g after 250 cycles under a high rate 2.0 C. A 763 mAh/g discharge specific capacity of this sulfur nanosponge cathode (abbreviated as “SULFUN”) was obtained after 100 cycles under a rate of 0.2 C. 520 mAh/g and 290 mAh/g discharge capacities were attained after 300 and 500 cycles, respectively, making this cathode material attractive for powering portable electronics.

The surging demand for rechargeable batteries in portable electronics and electric vehicles has stimulated extensive studies on various lithium-based electrode materials^{1,2}. Sulfur is nontoxic and earth-abundant^{3,4}, it hosts two lithium ions non-topotactically, and exhibits a theoretical capacity of 1675 mAh/g, almost 10 times that of LiCoO_2 . In terms of gravimetric energy density, at 2.1 V versus Li/Li^+ , it is still 5 times that of LiCoO_2 . However, sulfur and its insoluble Li_2S_2

and Li_2S forms are poor electronic conductors. This necessitates a certain amount of excellent electron conductors like carbon to be coupled. Sulfur also does not conduct Li^+ ion very well, so intimate contact of liquid electrolyte with sulfur can be used to enhance the effective Li^+ conductivity in the electrode. This is a double-edged sword, however. Researchers have found that lithium-sulfur batteries show initially exceedingly high capacity⁵, but the capacity suffers rapid decay in cycling due to dissolution of soluble lithium polysulfides Li_2S_X ($4 \leq X \leq 8$) into bulk liquid electrolyte, and/or volume expansion induced mechanical failures and a degrading electronic conductivity⁶. Conventional sulfur cathode loses 96% of its active sulfur over just ~30 cycles. To retard this loss, strategies^{3,4} modifying the electrolyte⁷⁻¹¹, electrode^{12,13} and operating voltage¹⁴ have been proposed. Suo et al. used ‘Solvent-in-Salt’ electrolyte with ultrahigh salt concentration to achieve a high-energy rechargeable battery^{15, 16}. A strategy of inhibiting undesirable polysulfide dissolution reactions via modifying the charging condition was recently developed by Su et al.¹⁴ that leads to ultra-long cycle life (>500 cycles). Additives like graphene^{17, 18}, mesoporous carbon^{5, 19}, and conductive polymers²⁰⁻²⁴ were exploited to facilitate efficient electron conduction. And by encapsulating sulfur in TiO_2 nanoshells with pre-existing void, the ~80% volume expansion of sulfur in lithiation can be accommodated, so the battery could run over 1000 cycles¹². While recent progresses demonstrated promising enhancements in the performance²⁵, how to improve the cyclability and sulfur utilization by a cost-effective, simple and scalable synthesis is still in demand.

Here we exploit commercially available Conductive Carbon Blacks (such as Super P[®]) using a facile wet-chemistry method to synthesize a sulfur-carbon nanosponge, whose evolving microstructure in lithiation/delithiation helps to delay the loss of active sulfur and enhance the cyclability. Our strategy is to use cheap carbon black as the base matrix to construct a sulfur-covering-carbon sponge, instead of the traditional carbon-wrapping-sulfur geometry^{12, 17}. This may sound counter-intuitive, since sulfur is the phase one wants to protect from leaching, so in most nanostructuring strategies people tend to isolate sulfur from the liquid electrolyte by completely encapsulating it. Here it is not done.

In order to construct a well-blended matrix, a three-step process was developed: 1) Conductive Carbon Blacks such as Super P[®] was first functionalized using hydrochloric acid, as shown in Figure 1a. The carbon nanoparticles of ~70 nm in diameter adhere to each other, forming a percolating electrical network (Cnet, Figure 1a); 2) The as-grown small sulfur particles

surrounded with surfactants were dispersed on the matrix using an *in-situ* redox reaction under ultrasonic agitation or mechanical stirring (Figure 1b-c); The ultrasonic agitation will break apart carbon particle agglomerations, enabling *in-situ* forming of small sulfur-carbon clusters (2-4 μm), as shown in Figure 3c-d. For comparison, a well-mixed S/C composite via mortar milling without sonication displays separate, flat sulfur flakes with much larger sizes of 40-60 μm (Figure 3b). 3) With heating at an annealing temperature of 150°C or 200°C, the distributed sulfur was melted and deeply infiltrated into the framework to form a sulfur-covering-carbon configuration (Figures 1d and 3e-f). Since the melting temperature of sulfur is 115.2°C, the annealing would cause the sulfur particle to melt, wet and spread across the carbon surface, forming another percolating network (Snet). Cnet and Snet interpenetrate each other and are in intimate contact, forming a nanostructured sponge which we call SULFUN (See Experimental details in the Appendix). During lithiation/delithiation, the sponge-like structure of Cnet has the ability to breath to accommodate ~80% volume expansion of Snet without losing electrical contact, according to the porosity evaluation. SULFUN has a different initial topology (Cnet+Snet, with both initially open to the outside) from the carbon-wrapping-sulfur approach^{12, 17} where one aims to completely encapsulate and isolate the sulfur.

Battery performance of SULFUN was measured via coin cells, which were assembled inside a glove box. SULFUN was used as cathode while a Li foil served as anode, in an electrolyte of 1.0 M lithium bis-trifluoromethanesulfonylimide (LiTFSI) in 1,3-dioxolane (DOL) and 1,2-dimethoxyethane (DME) (DOL:DME=1:1 in volume). Because the Snet is initially open to the outside, the LiTFSI+DOL+DME liquid electrolyte wets and infiltrates Snet in the initial lithiation, dissolving some sulfur and forming some soluble lithium polysulfides. The “wet” Snet then has some significant Li^+ conductivity, that percolates within Cnet.

Figure 2a depicts an initial discharge specific capacity of ~1100 mAh/g at a 0.2 C rate (C rate is calculated based on the theoretical capacity 1675 mAh/g of sulfur). Two main plateaus appear in the discharging window of 2.5 to 1.5 V (Figure 2a). The first plateau (I) centering at ~2.3 V corresponds to the sequential reduction of sulfur (S_8) to high-order polysulfides Li_2S_X ($4 \leq X \leq 8$). During the complex reactions, a series of soluble lithium polysulfides are generated¹⁴. As illustrated in the discharge curve, this plateau is quite short, which only presents a minor capacity of ~165 mAh/g (about 15% of the overall 1100 mAh/g). Then there is a short transition (II), which contributes a small portion ~146 mAh/g (~13%) as well. Such fast reaction mitigates

the loss of sulfur by way of soluble polysulfides (the “shuttling effect”). A big plateau (III) is located at ~ 2.06 V, which is attributed to the continuous conversion of Li_2S_X ($4 \leq X \leq 8$) to low order Li_2S_2 and Li_2S . In this last step, sulfur is reduced to the final state of insoluble Li_2S ²⁶. The dominance of this reaction is evidenced by the long plateau which constitutes a major portion ($\sim 64\%$) of the total capacity. Although the insoluble sulfides can increase the volume and the electrical resistance²⁶, plenty of interlinked carbon nanoparticles maintain good electron conduction paths to ensure uninterrupted lithiation/delithiation. In other words, Cnet is mechanically robust enough and has nano-pore-like configuration (Specific surface area: >70 m^2/g) with flexibility that it can accommodate the $\sim 80\%$ volume change of Snet by unfolding, while maintaining good electrical conductivity and contact with Snet. Otherwise the cycling performance would degrade very rapidly, which was indeed the case historically¹².

Shown in Figure 2b (red) is the cycling capability of SULFUN cathode annealed at 200°C . With a charging/discharging rate of 0.2 C, a specific discharge capacity as high as ~ 763 mAh/g was retained after running 100 cycles. After 300 cycles, a ~ 520 mAh/g capacity was still retained, which implies less than 0.2% decay for each cycle (Figure 2b). The capacity was maintained at a high level of ~ 290 mAh/g even at the 500^{th} cycle. A long-cyclability coin cell made of the same matrix is shown in Figure S1, demonstrating reproducibility. Because of the multi-step procedure during material synthesis and battery assembly, a variation in performance inevitably exists. The 150°C annealed sample displays a better cycling behavior, as evidenced in Figure 2c. After being subjected to extremely long cycling such as 1500 cycles, the discharge capacity of one cell is still as high as 158 mAh/g (Figure 2c). It is noted that after running 1100 cycles, the capacity shows almost no big drop (Figure 2c inset). A comparison of battery performance using the current method with literature is shown in Table S1^{15, 27-31}.

For microstructural comparison, coin cells made of commercial pure sulfur and mortar-milled S/C mixture cathodes were also tested, as shown in Figures 2b and S1. For the pure sulfur, the capacity drastically decreased from ~ 856 mAh/g to less than 200 mAh/g after only 15 cycles. The battery almost died after 29 cycles. As for the mortar-milled S/C mixture, the capacity dropped to less than 300 mAh/g after 100 cycles and almost down to zero at the 200^{th} cycle (Figure 2b, blue). The two plateaus from the charge/discharge voltage profile almost disappeared after 200 cycles (Figure S3) while they were still observed apparently even after 1500 cycles in SULFUN (Figure S2). We further found that in the coin cell assembly of SULFUN cathode,

adding a trace of conductive polymer polypyrrole (PPy) in the SULFUN/binder/Super P slurry acts as a network to restrain the dissolution of intermediate products. It will not impair Li^+/e^- transport due to the relatively high electric conductivity (0.005 Scm^{-1}) of PPy. The ability to trap both polysulfides and the possibly detached sulfur particles without raising resistance can further deter the fast fading of capacity.

The morphology of sulfur was characterized by electron microscopy. As shown in Figure S4a, the as-fabricated sulfur without carbon host shows the size ranging 5-10 μm . The commercial sulfur after mortar milling displays the size ranging 40-60 μm (Figure 3a-b). However, during SULFUN fabrication step 2), the size of sulfur particles dispersed on the carbon matrix surface becomes smaller (Figures 3c-d and S5d-e). It reveals the sulfur particles with sizes of 2-4 μm , which is about 50% less than the free-standing sulfur in Figure S4a and much smaller than the commercial pure (Figure 4a) and mortar-milled (Figure 3a-b) sulfur. The sulfur was dispersed rather uniformly on the carbon surface, as illustrated from the energy-dispersive X-ray spectroscopy (EDS) mapping in Figures 3d and S5d. In contrast to the separate sulfur particles after milling (Figure 3a-b), the semi-closed ball-like S/C cluster with decreased sizes ensures a sufficient contact, leading to a high ion/electron conductivity (Figure 3c-d). In order to further reduce the microstructural length scale and form a compact nanoscale S-C network, the sulfur was subsequently melted during SULFUN fabrication step 3) at 150°C or 200°C, respectively. Under this temperature, like the water filtrating sponge, the fluidic sulfur permeated inside the sponge (Figure 1d). As displayed in Figures 3e-f and S4b-c, the sulfur almost cannot be isolated from the Cnet any more. TEM image of the 200°C treated sample also exhibits a uniform composition (Figure S5f). Elemental mapping of a local area clearly shows a proportional distribution of sulfur and carbon (Figures 3f and S5a-c). These data imply that Snet has been interfused with the nanostructured Cnet, with improved the adhesion between sulfur and carbon, providing a fast pathway for ion/electron transport. According to the estimated volume of matrix, the gravimetric loading of sulfur is about 70 wt%. Quantitative thermal-gravimetric analysis (TGA) reveals the actual loading of sulfur in SULFUN was 62-65 wt% (Figure S6).

The initial size of sulfur plays a critical role on the imbibition process and the later cyclability. To obtain a homogenous cathode, well-dispersed sulfur particles with a small size is significant. In the present modifications, Carbon Blacks first underwent acid treatment in

hydrochloride to create functional hydroxyl/carboxyl groups. In parallel, the added surfactant groups wrapped the fresh sulfur particles to prevent Ostwald ripening. They also made the sulfur particles more efficiently distributed over the framework. Then, a very important step is the extremely slow redox progress. The sodium thiosulfate solution was added into the functionalized carbon solution drop by drop with vigorous agitation. In this situation, sulfur with a reduced size uniformly spread over a wide area of the carbon surface, before they melt and spread further by annealing at 150°C with 50 hours or 200°C with 2.5 hours (Figure 3c-d). However, the commercial grinding and pure sulfur possesses much large sizes of 40-60 μm (Figures 3a-b and 4a-b).

Next, we investigated the morphological evolution of the electrode surface during lithiation/delithiation. As can be seen from Figure 4a, the surface of the original commercial sulfur is quite smooth. A clear boundary between sulfur and other materials like carbon and binder is observed via the elemental mapping (Figure 4b). However after only two cycles, several holes with size 2-4 μm were observed on sulfur particles, which by then were already severely deformed and shrunk, indicating a fast loss of the active sulfur (Figure 4c-d and Figure S7). The sulfur particles were dramatically deformed and broke into small particles which were dispersed among the surface inhomogeneously (Figure S7). In contrast, the surface of the SULFUN electrode is still smooth after the cycling, as shown in Figure 4e. The elemental mapping of sulfur indicates a homogeneous distribution (Figure 4f). From analysis of the cross-section of the pure sulfur electrode, O and F which can only be precipitated out from the electrolyte was found to be dispersed across the whole electrode film (~ 40 μm , Figure 5a), indicating deep invasion of the liquid electrolyte and corrosion of the sulfur. However, the O and F elements were highly concentrated at the top surface (1-2 μm) with the SULFUN electrode (Figures 5b and S8), indicating liquid electrolyte invasion and corrosion were probably repelled from the inside matrix. The corrosion reaction is believed to be heterogeneous and anisotropic, as illustrated in Figures 6a and S9a. Some locations will be more heavily corroded and consequently generate holes/cracks, causing the whole particle to split (Figure 6a). The electrode surface composed of pure or milled sulfur displays a larger solid-liquid interface S_{contact} to the liquid electrolyte but with a smaller volume of sulfur V_s (Figure 6b and Figure S9a). In this case, the liquid electrolyte can easily permeate into the electrode (Figure 5a), which also creates a path to carry away the soluble polysulfides. However, the compactly nanostructured SULFUN

exposes only a very small area of naked sulfur to the liquid electrolyte (Figures 6c and S9b) limiting the sulfur dissolution, even when the intermediate lithium polysulfides are formed inside. Here a possible mechanism is suggested. Because the Snet is initially open to the outside, the LiTFSI+DOL+DME liquid electrolyte wets and infiltrates Snet in the initial lithiation, dissolving some sulfur and forming some soluble lithium polysulfides. The “wet” Snet then has some significant Li⁺ conductivity, that percolates within Cnet. However, once the embedded sulfur on the top is “flown away”, the carbon nanoparticles remaining (tens to hundreds nanometers, as shown in Figures 5b and S8) will possibly concentrate to form a rather dense carbon-rich layer as a passivation layer against corrosion, which serves like a sieve to selectively block larger molecules such as the electrolyte and polysulfide while allowing small Li⁺/e⁻ to pass through (Figures 6c and S9). In this regard, the carbon-based interlayer architecture built by Su et al. probably has a similar polysulfide-blocking function¹⁴.

An additional carbon layer with tens of μm thickness was coated on the SULFUN surface. Figure 7 shows the cycling performance and coulombic efficiency of the modified SULFUN battery at different charge/discharge rates. As can be seen from Figure 7a, an initial >1300 mAh/g capacity was achieved and then was maintained at a value of ~1100 mAh/g until 60 cycles, accompanying with the coulombic efficiency >98%. Under the 10 times faster charging/discharging (2.0 C), a special discharge capacity of ~400 mAh/g was still attained after 250 cycles (Figure 7b). This high rate capability indicates the extra carbon can act as a passivation layer to reduce the “shuttling effect”, as the *in-situ* formed carbon-rich passivation layer on SULFUN surface, leading to a long battery life.

To better understand the selective permeation effect, we calculate the size dependence of the molecule/ion on the solubility and diffusion coefficient inside the Super-P. The mass transport flux is proportional to the product of the solubility and the diffusion coefficient in carbon black, as³²⁻³⁴

$$J \sim \frac{k_B T}{6\pi M^{1/2} a} \exp\left(-\frac{Q}{k_B T}\right) \quad (1),$$

where k_B is the Boltzmann constant, T is temperature, M and a are the mass and the average radius of the molecule/particle, respectively. Q is the effective activation energy, combining both insertion energy and migration energy barrier. When a molecule/ion in the liquid electrolyte is

inserted into and diffuses inside the passivation layer, both interfacial and elastic energies contribute to Q .³⁵

$$Q \approx F_{\text{surface}} + F_{\text{elastic}} = 4\pi a^2 \gamma + \frac{24\pi a^3 \mu K \varepsilon^2}{3K + 4\mu} \quad (2),$$

where γ is the interfacial energy, K , μ and ε are the bulk modulus, shear modulus and dilatational misfit strain, respectively. For small particles such as single lithium ion, molecular sulfur /polysulfide ion, or even electrolyte, $F_{\text{surface}} \gg F_{\text{elastic}}$, and eq. (2) becomes $Q \approx S\gamma$. Here, S is the surface area. The average surface energy of SuperP is $\sim 100 \text{ mJ/m}^2$ ^{36, 37} and the surface area of Li ion, small sulfur molecules S_4 and S_8 can be estimated using lithium ion radius of 1.34 \AA and the bond length values of various small sulfur molecules³⁸. Thus, we obtain from eq. (1) and (2) the ratio of permeation fluxes $J(X)$ ($X=\text{Li}, S_4, S_8$) as $J(\text{Li}):J(S_4):J(S_8)=1:10^{-3}:10^{-8}$, showing the permeation of the S_8 cluster is eight orders of magnitude slower than Li. The upshot of the above rough estimation is that a pure carbon layer (blocking the invasion of the liquid electrolyte into Snet) can selectively allow Li^+/e^- to easily get in, but prevent the larger polysulfides Li_2S_X ($4 \leq X \leq 8$) from getting in or out, thus slowing down the shuttling effect⁶ and act as passivating molecular sieve. Also, the fine-meshed Cnet will probably restrain and block much smaller sulfur particles from breaking off Snet mechanically and convecting into the liquid, even with certain degree of heterogeneous corrosion. In other words, the SULFUN nanocomposite can better facilitate stress relaxation and enhance flaw tolerance, which is maybe a generic behavior of nano-scale electrode materials.

In conclusion, the *in-situ* synthesized sulfur-carbon nanosponge using Conductive Carbon Blacks as a host greatly slowed down the loss of sulfur, hereby displaying a better cycling performance while maintaining a high capacity. The suggested passivation layer or extra carbon layers can prevent the decay of capacity by limiting the transport of the larger polysulfides Li_2S_X ($4 \leq X \leq 8$) without slowing down Li^+/e^- . This “defense-in-depth” strategy is distinct from the complete encapsulation or the “defense-in-perimeter” strategy most researchers have employed. Our improved coin-cell scale performance indicates that the polysulfides shuttling effect is ameliorable through nanostructural design and engineering. The high capacity, long cyclability, cheap raw materials and simple preparation make the SULFUN cathode material a potential candidate on the scale of industrial production.

Acknowledgements

We acknowledge the support by NSF grant DMR-1120901. JJN thanks Dr. Xiaofeng Qian for discussions.

Additional information

Supplementary information accompanies this paper at [xxxxxx](#). Reprints and permission information is available online at [xxxxxx](#). Correspondence and requests for materials should be addressed to J.L (email: liju@mit.edu).

Figure captions

Figure 1 Schematic of the *in-situ* synthesis of SULFUN matrix.

Figure 2 Discharge voltage profiles of SULFUN matrix. Discharge voltage profile of the matrix treated at 200°C with 2.5 hours at a rate of 0.2 C a). Cycling performance of commercial pure sulfur (green), mortar milled S/C mixture (blue), and SULFUN matrix (red) treated under 200°C for 2.5 hours b) and 150°C for 50 hours c) at a rate of 0.2 C.

Figure 3 SEM images and the corresponding Energy-dispersive X-ray spectroscopy (EDS) mappings. SEM morphology of the milled S/C mixture a). SEM morphologies of the SULFUN matrix before c) and after e) annealed at 200°C with 2.5 hours. b), d) and f) Sulfur and carbon mapping of the areas shown in a), c) and e), respectively.

Figure 4 Morphology evolution of commercial sulfur particle and SULFUN during the charge/discharge. SEM morphologies of the commercial sulfur mixture with SuperP and binder before a) and after c) cycling two rounds. b) and d) EDS Element mappings of the area shown in a) and c), respectively. e) SEM morphology of the electrode made of the SULFUN annealed at 200°C with 2.5 hours after two cycles. f) The corresponding sulfur element mapping from e).

Figure 5 Cross-section diagnosis of the electrode after two charge/discharge cycles. SEM images and the corresponding EDS element mappings of the cross-section of the electrode made of commercial sulfur a) and SULFUN b). The mapping data indicate that the electrolyte was suppressed by the SULFUN surface instead of the commercial sulfur.

Figure 6 Schematic of the reaction mechanism during the charging/discharging. a) The sulfur particle generates holes/cracks due to the anisotropic reaction. The commercial sulfur

particle shows a much larger S_{contact}/V_s ratio b) compared to the compact SULFUN matrix c), which greatly delays the loss of sulfur.

Figure 7 Cycling performance of modified SULFUN coin cells at the different charge/discharge rates. The cyclability of batteries made of SULFUN coated with an additional carbon layer at 0.2 C with coulombic efficiency a) and at 2.0 C b), respectively. 0.1 M LiNO_3 was added into the electrolyte solution.

Supplementary Figures

Table S1 The battery performance of different Li/S battery systems.

Figure S1 Comparable cycling performance of the pure sulfur and SULFUN matrix treated under 200°C with 2.5 hours at a rate of 0.2 C. The inset is the enlarged cycling profile. This sample was synthesized using the complete method as in Figure 2b.

Figure S2 Charge/discharge voltage profiles of the SULFUN coin cells after cycling at 0.2 C. Samples annealed at 200°C a-b) and at 150°C c-d).

Figure S3 Charge/discharge voltage profiles of the mortar milled S/C mixture coin cells after cycling at 0.2 C. The 1st a) and the 200th b) cycles.

Figure S4 SEM imaging of as-synthesized pure sulfur without carbon a), SULFUN matrix treated at 150°C for 50 hours b), and 200°C for 2.5 hours c). Scale bar is 1 μm .

Figure S5 EDS mappings and electron microscopy imaging of the SULFUN matrix. a) SEM morphology of the matrix annealed at 150°C with 50 hours. Carbon b) and sulfur c) mappings of the area shown in a). d) Sulfur and carbon mapping of as-received SULFUN matrix before heating. TEM imaging of the SULFUN before e) and after f) heating at 200°C with 2.5 hours. Scale bar in e) and f): 5 μm .

Figure S6 TGA profiles and DTA curves recorded in argon with a heating rate of 10°C min^{-1} , for SULFUN matrices treated at 150°C with 50 hours a) and 200°C with 2.5 hours b), respectively.

Figure S7 SEM image and EDS mapping of the commercial cathode electrode after running two cycles. a) SEM morphology of the electrode. b) The corresponding sulfur element mapping.

Figure S8 SEM image and the corresponding EDS element mapping of the cross-section of the electrode made of SULFUN after charging/discharging two cycles (different sample with Figure 5b). The dashed white shows the boundary between the newly formed carbon layer and the electrode film.

Figure S9 Illustration of the reaction mechanism during the charging/discharging. a) The commercial sulfur particle exhibits more pathways of lithium polysulfide/electrolyte contact, while b), the generated carbon-rich layer reduces the solid (matrix)/liquid (electrolyte) interface thus prevents the major loss of active material sulfur.

Experimental details

In-situ synthesis of S-C sponge matrix

Details of the *in-situ* synthesis of Sulfur-Carbon sponge matrix are as follows. 70 wt% (according to the approximate loading in the final S-C matrix) Conductive Carbon Blacks (Super C65, Timical) was first treated in a solution mixed with 20 ml hydrochloric acid (1 N volumetric solution, Avantor Performance Materials, Inc.) under stirring on a hot plate (Super-Nuova, Thermo Scientific) for 2 hours at 70°C. Then 100 ml deionized water was added. Meanwhile, sodium thiosulfate (anhydrous, 99%, Alfa Aesar) was dissolved in 150 ml deionized water with surfactant Triton X-100 (1% in deionized water, Alfa Aesar)¹⁷. Then, the sodium thiosulfate solution was added into the Conductive Carbon Blacks solution with a dropping speed of ~1 ml/min under an ultrasonic agitation (Symphony, VWR Ultrasonic Cleaner) at a constant temperature of 70°C. The reacted sample was centrifuged (IEC HN-S II Centrifuge, Damon/IEC Division) and dried at 60°C in an oven (Symphony, VWR). Finally, the dried mixture was annealed at temperatures of 150°C for 50 hours (“low-temperature”) or 200°C for 2.5 hours (“high-temperature”) in air, respectively. The collected samples were stored for coin cell assembly and battery performance test.

For comparison, 80 wt% commercial sulfur (Sulfur powder, 99.5%, Alfa Aesar), 10 wt% Super P and 10 wt% binder were uniformly milled for 30 minutes in a mortar. After the milling, the mixture was applied to make a slurry on Al foil and then the final coin cell was assembled using a same protocol.

Characterizations of morphology, chemical composition, and structure

SEM: The surface morphologies were checked by FEI/Philips XL30 FEG Environmental Scanning Electron Microscope (ESEM) and JEOL 6320 Field-Emission High-Resolution SEM at 5-10 kV incident energy. The carbon-sulfur elemental mapping was obtained through energy-dispersive spectroscopy microanalysis using an INCA EDS detector at 20 kV acceleration voltage.

TEM: The as-grown sulfur and S-C sponge treated at different annealing temperatures were characterized by transmission electron microscopy (TEM) using a JEOL JEM-2010F at an

accelerating voltage of 200 kV. The TEM sample was dispersed on a lacy carbon film supported on a copper grid to acquire the images. In order to reduce electron-beam damage, a low magnification with weak beam intensity was applied when the images were captured.

TGA: Thermal gravimetric analysis (TGA, SEIKO SSC/5200 TG/DTA220 thermal analysis station) and differential scanning calorimetry curves were recorded in argon as working gas. The temperature program was set to be isothermal at 50°C for 10 min and heated up to 650°C with a heating rate of 10°C min⁻¹.

Assembling coin cell and testing battery performance

Battery behavior of the synthesized material was performed via a coin cell. Typically, a CR2032 coin cell (MTI) with a lithium foil as counter/reference electrode was assembled in an argon-filled glove box (LABmaster SP, MBraun) with both O₂ and H₂O concentrations were lower than 0.1 ppm. The Celgard 2400 was used as the separator. For liquid electrolyte, we used the typical 1.0 M lithium bis-trifluoromethanesulfonylimide in 1,3-dioxolane and 1,2-dimethoxyethane (volume ratio 1:1, Novolyte). All of the battery performances were tested without additives except the rate data shown in Figure 7. A hydraulic crimping machine (MSK-110, MTI) was employed to close the cell. To make a slurry, the active material of sulfur-SuperP sponge, or pure sulfur synthesized using a same method but without carbon, or milled sulfur/carbon mixture was blended with 10 wt% Super C65 (Timical), 10 wt% poly (vinylidene fluoride) binder (MTI), and a small amount of polypyrrole solution (polypyrrole doped, 5 wt% dispersion in H₂O, conductivity of dried cast film: >0.0005 S/cm, Sigma-Aldrich) dissolved in N-methylpyrrolidone (MTI). The sulfur loading was designed to be 1.0 mg/cm² for 150°C sample and 2.0 mg/cm² for 200°C sample, respectively. The mixture was sonicated until a homogeneous slurry was formed. Then the slurry was coated onto aluminum foil current collector. After drying 2 hours at 90°C in an oven, the sample was cut to serve as cathode.

For the high-rate charge/discharge test, an additional layer which is composed of carbon/binder was coated on the top of the dried slurry made of SULFUN. In a typical experiment, the melted sulfur/carbon mixture with 10 wt% SuperP and 10 wt% poly (vinylidene fluoride) binder was first coated on the aluminum foil, as described above. After the first slurry was almost dried, the secondary slurry composed of SuperP (80 wt%) and binder (20 wt%) with

a loading of $\sim 2.0 \text{ mg/cm}^2$ was coated on the surface. Then the sample was dried overnight at 65°C in an oven for battery assembling.

The packed coin cell was galvanostatically charged/discharged in a fixed voltage window between 1.4 and 2.5/2.8 V on a 12-channel Arbin Instruments BT2000 battery tester at room temperature. The cycling capability was recorded at a charging/discharging rate of 0.2 C and 2.0 C, respectively. The discharge specific capacity was calculated based on the actual sulfur loading corrected by the TGA test.

References

1. P. G. Bruce, S. A. Freunberger, L. J. Hardwick and J. M. Tarascon, *Nat. Mater.*, 2012, **11**, 19-29.
2. R. Van Noorden, *Nature*, 2013, **498**, 416-417.
3. A. Manthiram, Y. Z. Fu and Y. S. Su, *Accounts Chem. Res.*, 2013, **46**, 1125-1134.
4. Y. X. Yin, S. Xin, Y. G. Guo and L. J. Wan, *Angew. Chem.-Int. Edit.*, 2013, **52**, 13186-13200.
5. X. L. Ji, K. T. Lee and L. F. Nazar, *Nat. Mater.*, 2009, **8**, 500-506.
6. Y. V. Mikhaylik and J. R. Akridge, *J Electrochem Soc*, 2004, **151**, A1969-A1976.
7. Z. Lin, Z. C. Liu, W. J. Fu, N. J. Dudney and C. D. Liang, *Angew. Chem.-Int. Edit.*, 2013, **52**, 7460-7463.
8. E. Peled, Y. Sternberg, A. Gorenshtein and Y. Lavi, *J Electrochem Soc*, 1989, **136**, 1621-1625.
9. S. E. Cheon, K. S. Ko, J. H. Cho, S. W. Kim, E. Y. Chin and H. T. Kim, *J Electrochem Soc*, 2003, **150**, A800-A805.
10. L. X. Yuan, J. K. Feng, X. P. Ai, Y. L. Cao, S. L. Chen and H. X. Yang, *Electrochem Commun*, 2006, **8**, 610-614.
11. J. H. Shin and E. J. Cairns, *J Power Sources*, 2008, **177**, 537-545.
12. Z. W. Seh, W. Li, J. J. Cha, G. Zheng, Y. Yang, M. T. McDowell, P.-C. Hsu and Y. Cui, *Nature Communications*, 2013, **4**, 6.
13. J. Wang, S. Y. Chew, Z. W. Zhao, S. Ashraf, D. Wexler, J. Chen, S. H. Ng, S. L. Chou and H. K. Liu, *Carbon*, 2008, **46**, 229-235.
14. Y. S. Su, Y. Z. Fu, T. Cochell and A. Manthiram, *Nature Communications*, 2013, **4**, 2985.
15. L. M. Suo, Y. S. Hu, H. Li, M. Armand and L. Q. Chen, *Nature Communications*, 2013, **4**.
16. Y. Sun, L. Zhao, H. L. Pan, X. Lu, L. Gu, Y. S. Hu, H. Li, M. Armand, Y. Ikuhara, L. Q. Chen and X. J. Huang, *Nature Communications*, 2013, **4**.
17. H. L. Wang, Y. Yang, Y. Y. Liang, J. T. Robinson, Y. G. Li, A. Jackson, Y. Cui and H. J. Dai, *Nano Lett*, 2011, **11**, 2644-2647.
18. M. K. Song, Y. G. Zhang and E. J. Cairns, *Nano Lett*, 2013, **13**, 5891-5899.
19. N. Jayaprakash, J. Shen, S. S. Moganty, A. Corona and L. A. Archer, *Angew. Chem.-Int. Edit.*, 2011, **50**, 5904-5908.
20. Y. Z. Fu and A. Manthiram, *Rsc Adv*, 2012, **2**, 5927-5929.
21. X. Liang, Y. Liu, Z. Y. Wen, L. Z. Huang, X. Y. Wang and H. Zhang, *J Power Sources*, 2011, **196**, 6951-6955.
22. H. K. Song and G. T. R. Palmore, *Adv Mater*, 2006, **18**, 1764-+.
23. J. L. Wang, J. Yang, J. Y. Xie and N. X. Xu, *Adv Mater*, 2002, **14**, 963-+.
24. Y. Yao, N. Liu, M. T. McDowell, M. Pasta and Y. Cui, *Energ Environ Sci*, 2012, **5**, 7927-7930.
25. G. Y. Zheng, Y. Yang, J. J. Cha, S. S. Hong and Y. Cui, *Nano Lett*, 2011, **11**, 4462-4467.
26. C. Barchasz, F. Molton, C. Duboc, J. C. Lepretre, S. Patoux and F. Alloin, *Anal Chem*, 2012, **84**, 3973-3980.
27. J. Schuster, G. He, B. Mandlmeier, T. Yim, K. T. Lee, T. Bein and L. F. Nazar, *Angew. Chem.-Int. Edit.*, 2012, **51**, 3591-3595.

28. C. F. Zhang, H. B. Wu, C. Z. Yuan, Z. P. Guo and X. W. Lou, *Angew. Chem.-Int. Edit.*, 2012, **51**, 9592-9595.
29. G. Y. Zheng, Q. F. Zhang, J. J. Cha, Y. Yang, W. Y. Li, Z. W. Seh and Y. Cui, *Nano Lett*, 2013, **13**, 1265-1270.
30. W. Weng, V. G. Pol and K. Amine, *Adv Mater*, 2013, **25**, 1608-1615.
31. S. Xin, L. Gu, N. H. Zhao, Y. X. Yin, L. J. Zhou, Y. G. Guo and L. J. Wan, *J Am Chem Soc*, 2012, **134**, 18510-18513.
32. R. B. Bird, *New York*, 1960, **Wiley**.
33. J. L. Anderson and C. C. Reed, *J Chem Phys*, 1976, **64**, 3240-3250.
34. A. Dondos and H. Benoit, *Polymer*, 1977, **18**, 1161-1162.
35. F. S. HENRY EHRENREICH, *SOLID STATE PHYSICS: Advances in Research and Applications, Vol. 59*, ELSEVIER ACADEMIC PRESS, 2004.
36. M. L. GonzalezMartin, B. Janczuk, L. LabajosBroncano and J. M. Bruque, *Langmuir*, 1997, **13**, 5991-5994.
37. J.-B. Donnet, R. C. Bansal and M.-J. Wang, *Carbon black : science and technology*, Dekker, New York, 1993.
38. B. Meyer, *Chem Rev*, 1976, **76**, 367-388.

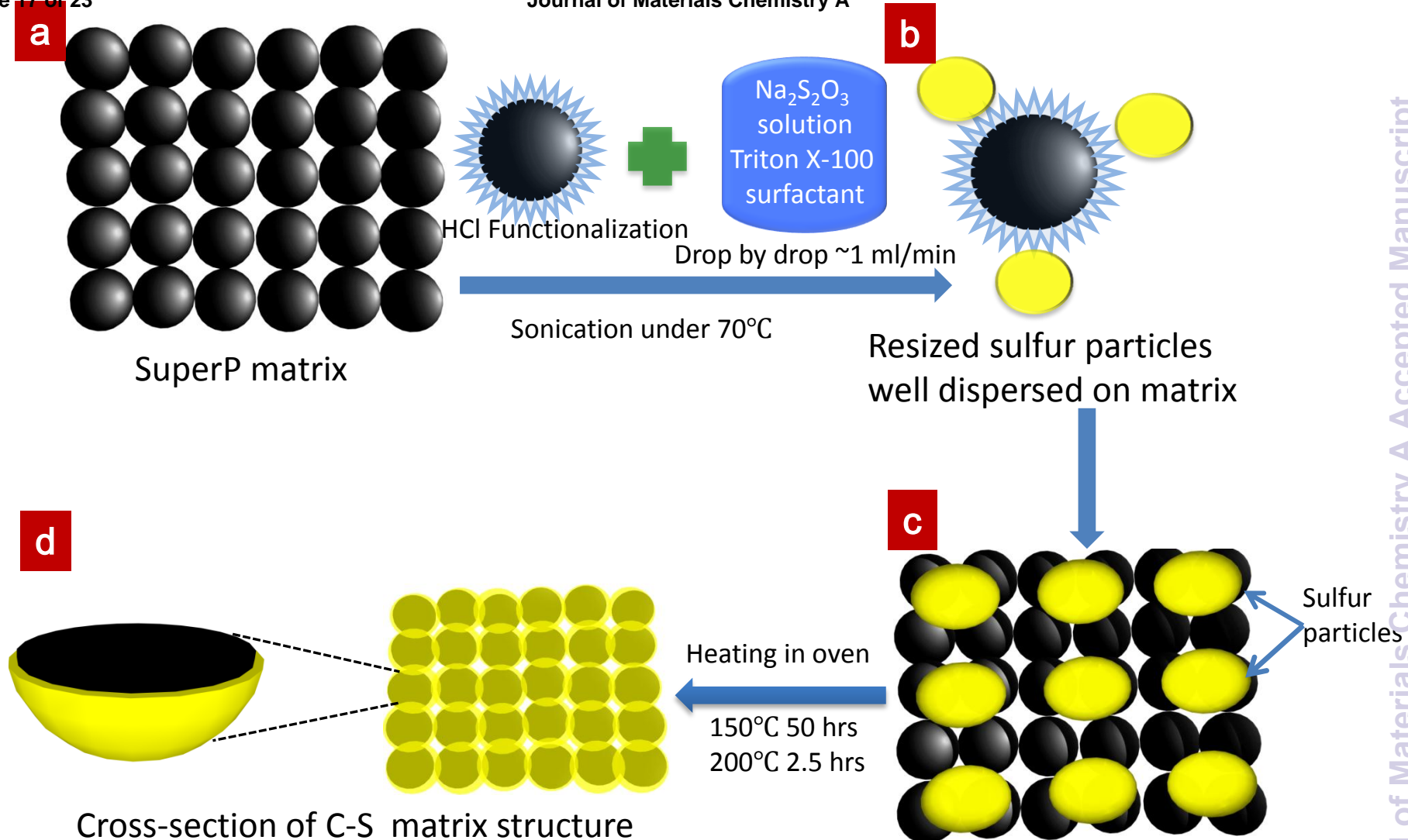


Fig. 1

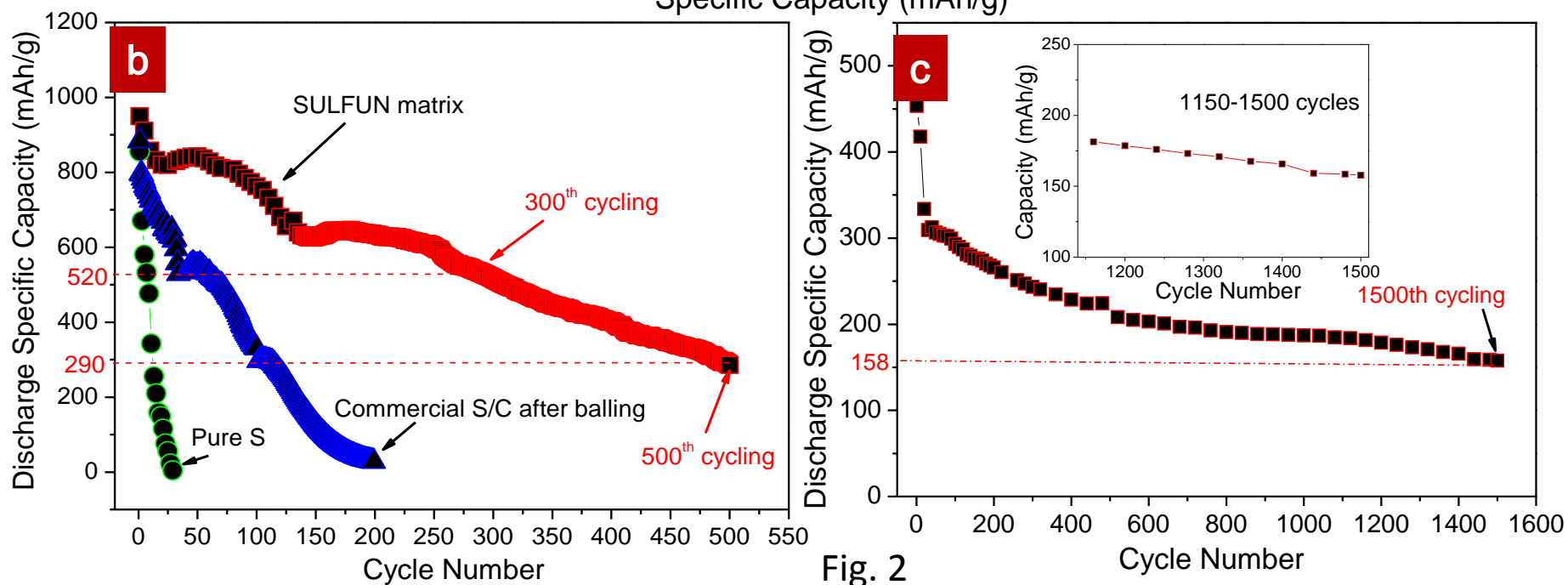
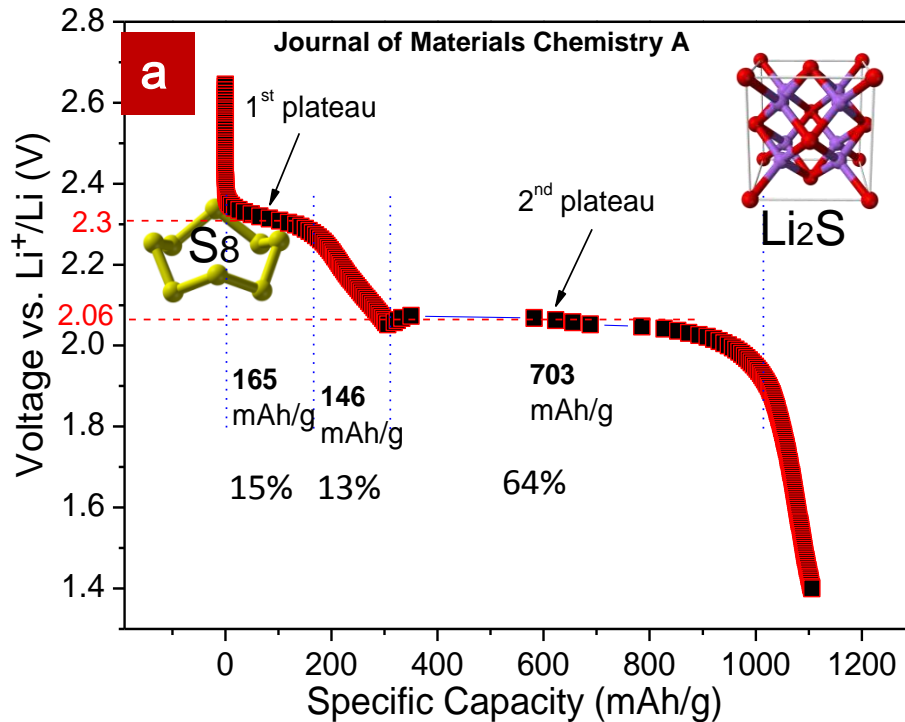


Fig. 2

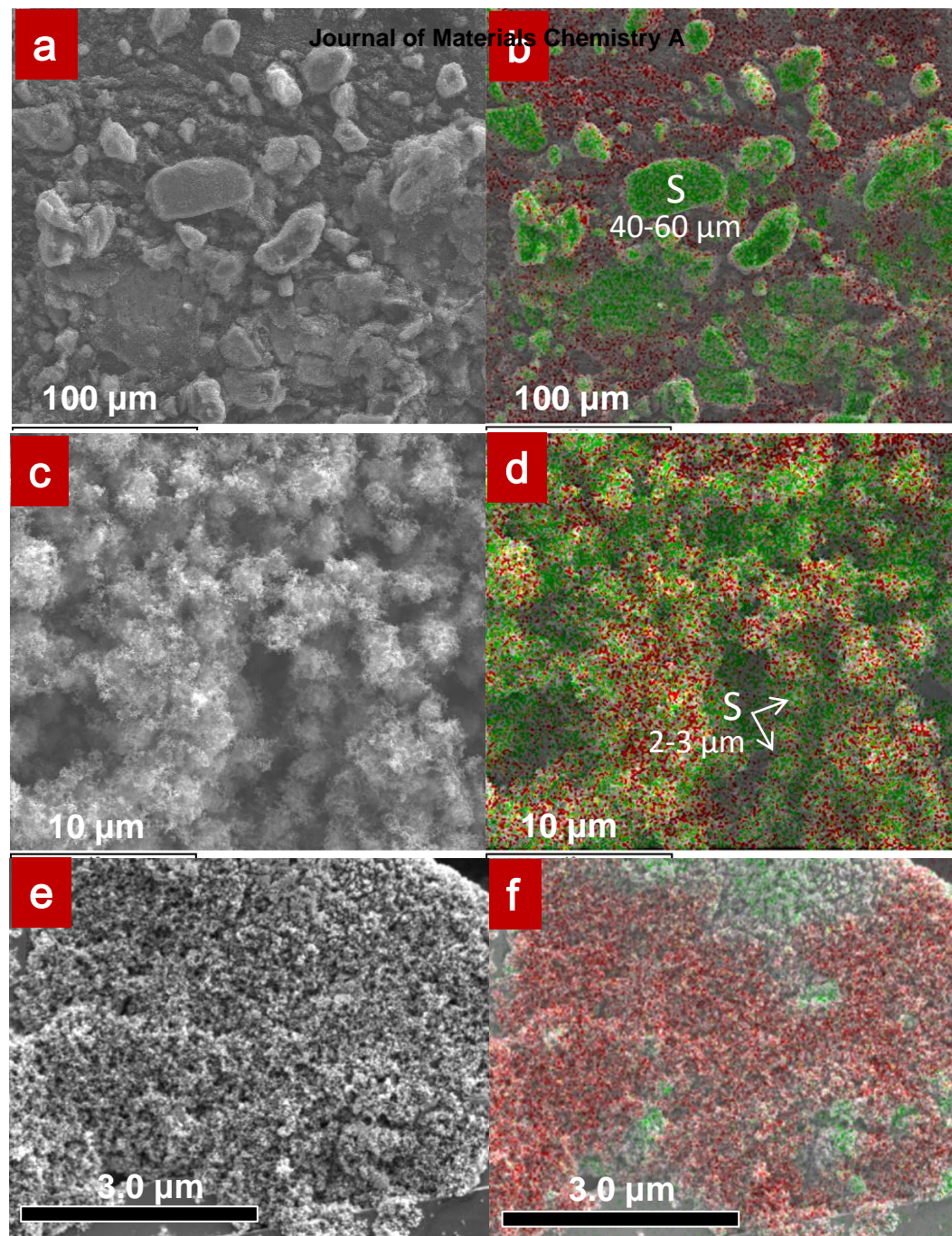


Fig. 3

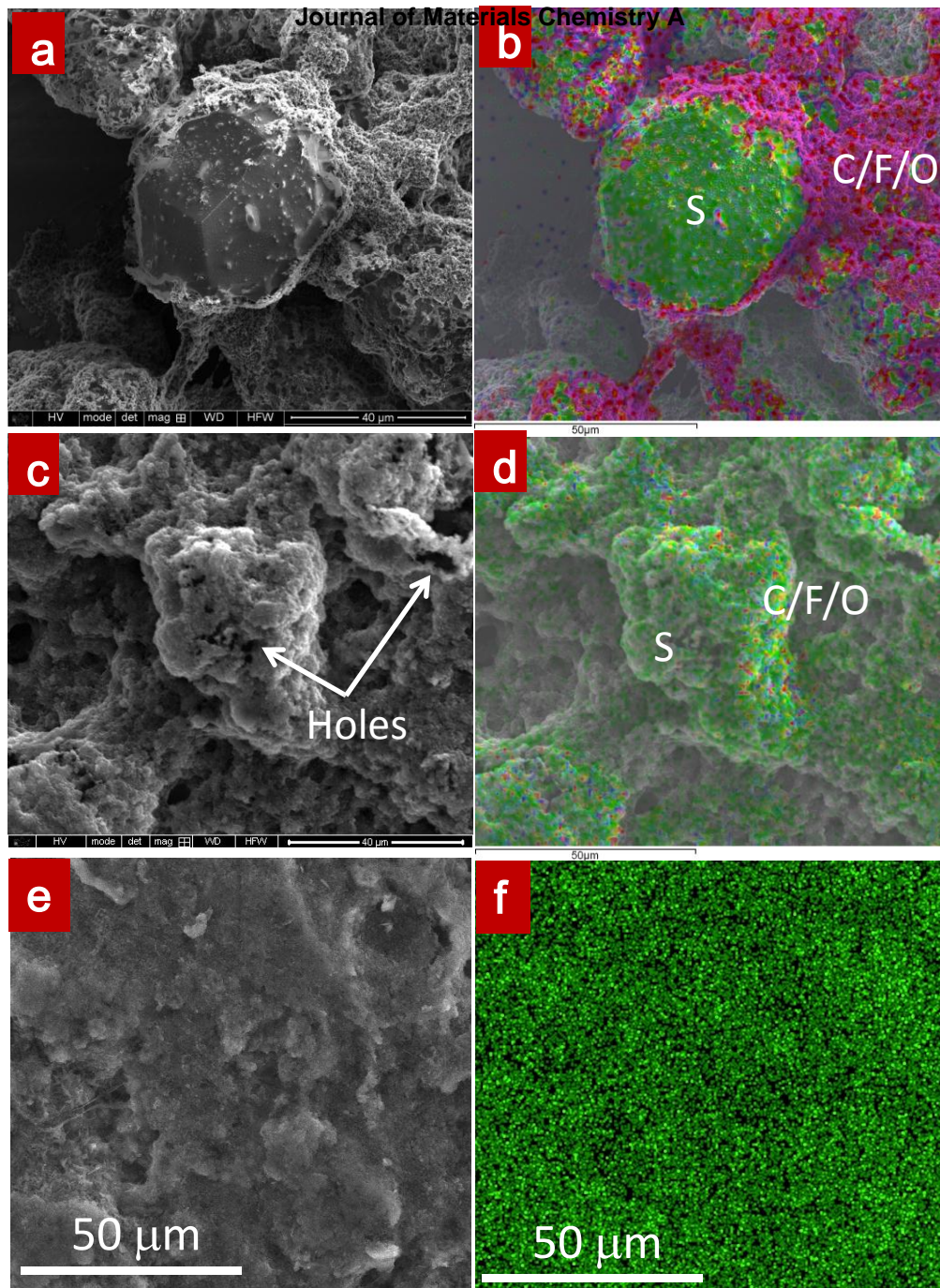


Fig. 4

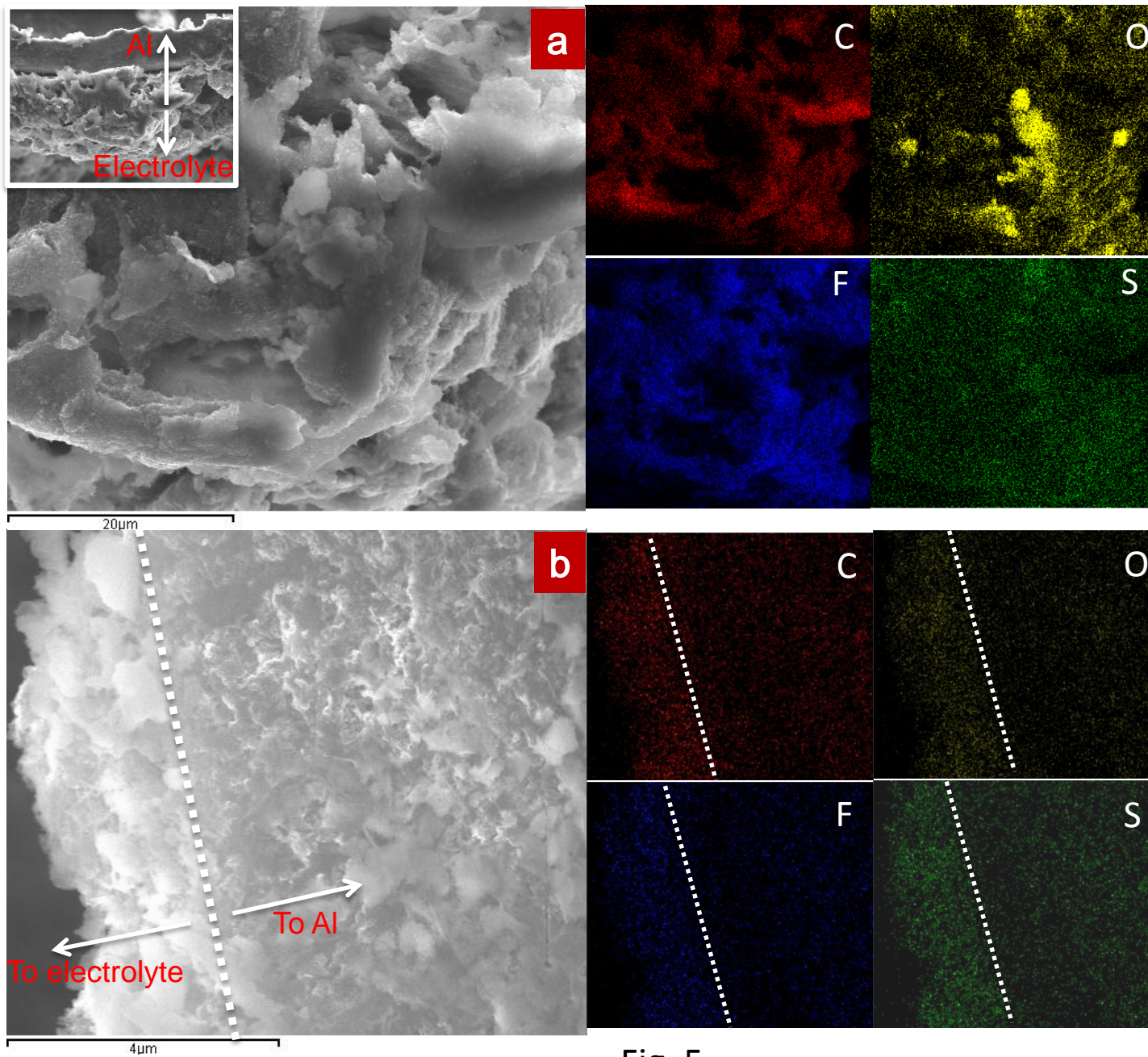
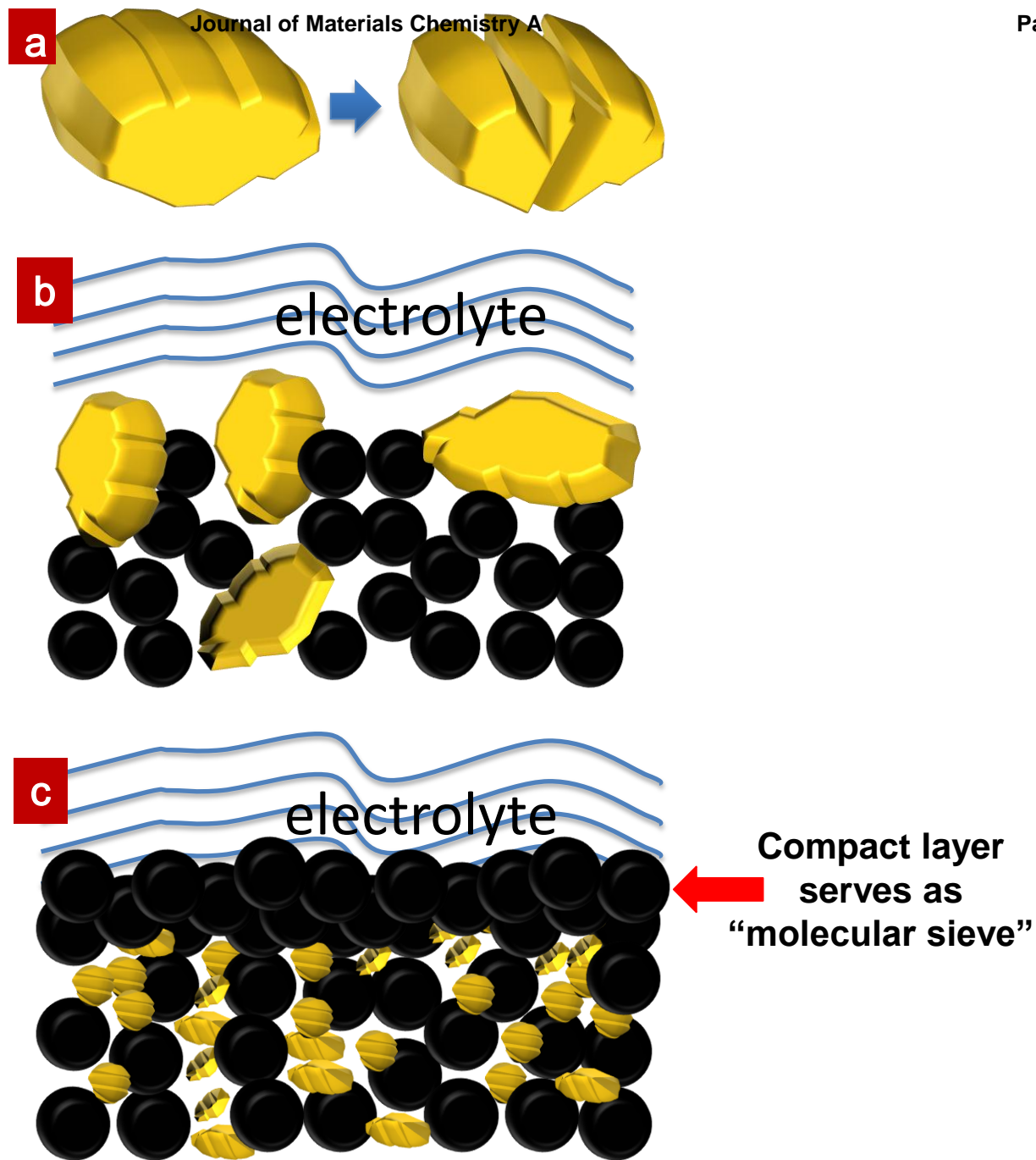


Fig. 5



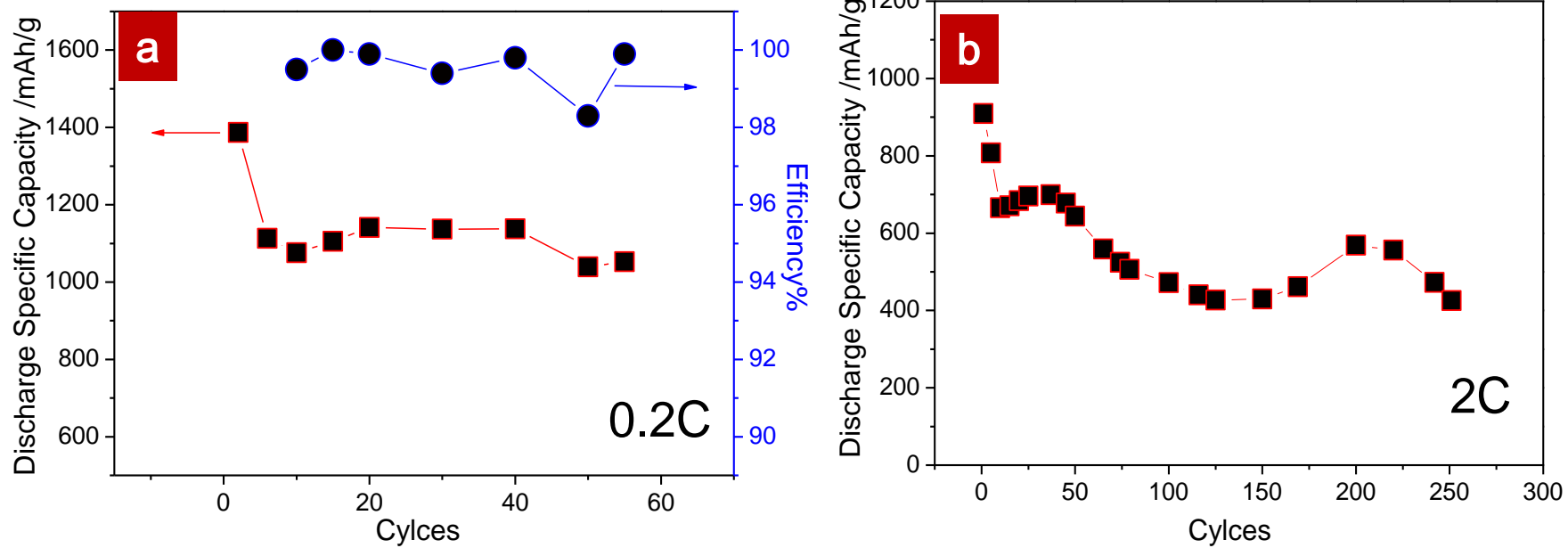


Fig. 7